Miner Deposita (2003) 38: 312–326
DOI 10.1007/s00126-003-0348-1

ARTICLE

Giorgio Garuti · Evgeny V. Pushkarev
Federica Zaccarini · Roberto Cabella · Elena Anikina

Chromite composition and platinum-group mineral assemblage in the Uktus Uralian-Alaskan-type complex (Central Urals, Russia)

Received: 12 February 2001 / Accepted: 17 December 2002 / Published online: 12 March 2003

Abstract Chromitite segregations in dunites of the Uktus Uralian-Alaskan-type complex (Central Urals, Russia) display large variation of the chromite composition: $Cr/(Cr+Al) = 0.46–0.77$, $Fe^{2+}/(Fe^{2+}+Mg) = 0.28–0.66$, and $Fe^{3+}/(Fe^{3+}+Fe^{2+}) = 0.23–0.59$. Three types of PGM assemblages have been recognized, varying in accordance with chromite composition: type I, dominated by Ru–Os–Ir (sulfides), is associated with magnesiochromite having $Fe^{3+}/(Fe^{3+}+Fe^{2+}) < 0.30$, in the southern dunite body. Type II, containing abundant Pt–Ir (alloys, minor sulfides), is found in magnesiochromite with $Fe^{3+}/(Fe^{3+}+Fe^{2+}) = 0.40–0.44$; type III, consisting of Ir–Rh–Pt–Pd (alloys, sulfarsenides, antimonides) in Fe-rich chromite having $Fe^{2+}/(Fe^{2+}+Mg) = 0.66$ and $Fe^{3+}/(Fe^{3+}+Fe^{2+}) = 0.59$. Positive anomalies of Ir and Pt, and a negative peak of Ru characterize the PGE patterns of chromitites with type II and III PGM assemblages, whereas a positive Pt anomaly is observed in their dunite host. Intensive fractionation of Pt–Fe alloys in the Uktus chromitites reflects the anomalous behavior of Pt which is decoupled from Rh and Pd. Among other factors, the high iron activity and oxygen fugacity in the parent melt appear to exert a major control on precipitation of Pt–Fe alloys, below sulfur saturation. The strong Pt anomaly in chromitites from Uktus may indicate that Uralian-Alaskan-type magmas were derived from a Pt-rich mantle source.

Editorial handling: O. Thalhammer

G. Garuti (✉) · F. Zaccarini
Dipartimento di Scienze della Terra, Universitá di Modena e Reggio Emilia, via S. Eufemia 19, 41100 Modena, Italy
E-mail: garutig@unimo.it

E.V. Pushkarev · E. Anikina
Ural Branch, Russian Academy of Sciences, Str. Pochtovy per 7, 620151 Ekaterinburg, Russia

R. Cabella
Dipartimento per lo Studio del Territorio e delle sue Risorse, Università di Genova, Europa 26, 16132 Genova, Italy

Keywords Urals · Russia · Chromite · PGE mineralization · Uktus · Uralien-Alaskan type

Introduction

Since the end of the 19th century it was realized that dunites and related chromitites from concentrically zoned complexes of the Uralian-Alaskan type were the major contributors of platinum in large placer deposits occurring in the so-called Platinum Belt of the Urals (Fig. 1; Betekhtin 1961; Razin 1976; Cabri and Genkin 1991 and references therein). In recent times, comparative study of PGE mineralogy in lode and placer deposits has provided support to this conclusion and showed that Pt–Fe alloys accompanied by Ir phases represent the most abundant constituents of the PGM assemblage (Cabri et al. 1996; Makeyev et al. 1997; Garuti et al. 2002; Malitch and Thalhammer 2002). Such a mineralogical specialization is remarkably consistent with geochemical data showing positive anomalies of Pt or Pt plus Ir as distinctive features of the chondritic PGE distribution patterns of Uralian-Alaskan-type dunites and chromitites from all over the world (Fominykh and Kvostova 1970; St. Louis et al. 1986; Malitch 1990; Nixon et al. 1990; Lazarenkov and Malitch 1991; Tistl 1994; Garuti et al. 1997b). These observations reflect an anomalous behavior of Pt which still remains poorly understood. In particular, the fractional decoupling of Pt from Rh and Pd is in contrast with mechanisms commonly expected for fractionation of PGEs in magmatic processes (Barnes et al. 1985). Furthermore, the Pt enrichment in the Uralian-Alaskan-type chromitites is not related to the segregation of magmatic sulfides during chromite precipitation, as it has been established in Pt-Pd-rich chromitites from layered intrusions and ophiolite complexes (Naldrett and Von Gruenewaldt 1989).

In this article we give a detailed description of chromitites and related PGMs occurring in dunites of the

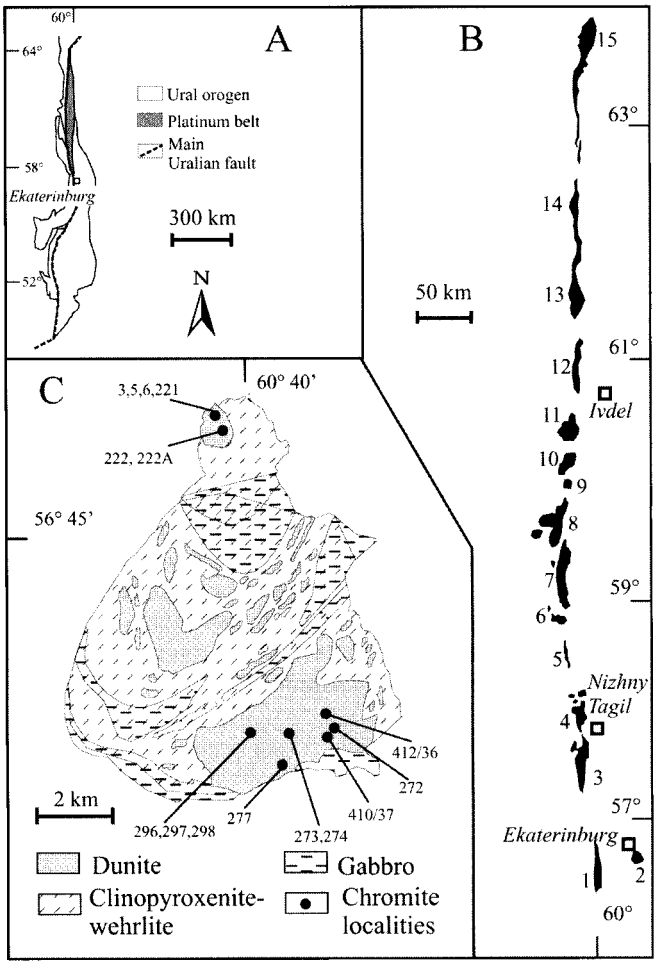

Fig. 1 **A** Geological setting of the "Platinum Belt" in the Ural orogen. **B** Geographical location of the major Alaskan-type massifs in the "Platinum Belt" of the Urals. *1* Revda, *2* Uktus, *3* Tagil, *4* Tagil Barancha, *5* Arbat, *6* Kachkanar, Pavda, *8* Kytlym, *9* Knyaspin, *10* Kumba, *11* Denezhk, *12* Pomursk, *13* Chistop, *14* Yalping-Niersk, *15* Khorasyur. **C** General geology of the Uktus complex and location of the investigated chromitite samples. The "UK" label of samples has been omitted for simplicity (modified after Pushkarev 2000)

concentrically zoned complex of Uktus (Central Urals). Mineralogical variations in the PGM assemblage and PGE distribution are strictly related with compositional changes in chromite and coexisting olivine, apparently consistent with variations in iron activity and oxygen fugacity during magmatic fractionation, at sulfur concentrations well below the level of saturation.

Geological setting and petrography of the Uktus complex

The Uktus complex (Pushkarev 2000) is located at the periphery of Ekaterinburg, about 50 km to the east of the southern end of the so-called Platinum Belt of the Urals (Fig. 1A, B). The complex covers an area of about 50 km^2 marked by positive gravity and magnetic anomalies, both having a sharp gradient along the external boundaries of the massif, suggesting that the Uktus body probably has a stock-like deep structure. The Uralian-Alaskan-type affinity of the Uktus complex was recognized since the early 1920s (Tokarev 1922), based on petrographic and structural similarities with Uralian-Alaskan-type complexes sensu stricto of the Urals, although it has been supported with petrologic data only recently (Pushkarev and Puchkova 1991; Pushkarev et al. 1994; Pushkarev 2000). However, some petrographic and geochemical features of the Uktus complex, namely, the absence of hornblendite–magnetite mineralization, and the overall low concentration in incompatible elements (K, P, Rb, Sr, and REEs) are atypical compared with classic Uralian-Alaskan-type intrusions of the Platinum Belt.

Dunite, clinopyroxenite, wherlite, olivine and amphibole gabbro are major constituents of the Uktus complex and characteristically lack orthopyroxene, as typical of Uralian-Alaskan-type intrusions (Taylor 1967). These lithologies are arranged in a concentrically zoned structure (Fig. 1C) in which dunite occurs embedded in a wherlite–clinopyroxenite envelope, passing outwards into gabbros. The composition of olivine varies from Fo_{96} to Fo_{75} and, as a rule, the Mg content decreases from the southern to the northern dunite body, and from core to rim in each dunite body. The core–rim transition is gradual and appears to be better developed in large dunite bodies compared with small ones. The dunites are variably serpentinized (10 to 60%) and contain accessory chromite which locally forms small vermicular aggregates and minor chromitite lenses and layers. Transition from dunite to clinopyroxenite is usually marked by the appearance of interstitial diopside in dunite, and abundant Fe-enriched olivine in clinopyroxenite. In some cases, the transition is marked by a zone with interlayered dunite and wehrlite. Clinopyroxenites consist of 90 to 80% clinopyroxene (diopside-augite), 10 to 20% olivine (Fo_{87}–Fo_{77}), and accessory pargasite (up to 5%) with subordinate magnetite and ilmenite. Two main types of gabbro are present. Olivine gabbro is composed of olivine (Fo_{75}–Fo_{68}), diopside, anorthite (An_{95}), titanomagnetite, ilmenite, and Ti-rich hornblende. It is found generally interlayered with clinopyroxenite in the cryptic, layered zone of the central part of the Uktus massif. Amphibole gabbro, composed of augite, labradorite (An_{60}) with accessory green hornblende, titanomagnetite, titanite and apatite, occurs as massive bodies in the central and southern parts of the massif. Accessory titanomagnetite (1.92–8.16 wt% TiO_2) enriched in V (0.69–1.24 wt% V_2O_3) and ilmenite, occurs as interstitial aggregates moulded on the silicates. Sulfide minerals are very scarce in the Uktus complex. In ultramafic rocks, they consist of secondary Ni-rich phases (heazlewoodite, millerite and pentlandite) resulting from late-stage removal of Ni from olivine during serpentinization. Accessory pyrrhotite, pentlandite and chalcopyrite commonly occur as minute blebs in gabbros, possibly indicating segregation of some sulfide liquid in the very late stages of magmatic fractionation.

The Uktus complex was probably emplaced in Early Cambrian times and, in the Upper Silurian to Devonian, underwent slow-cooling equilibration, deformation, followed by low-grade metamorphism, producing amphibole, serpentine, chlorite and epidote (Kaleganov and Pushkarev 1992; Pushkarev 2000).

Analytical methods

In all, 54 polished sections, obtained from 14 chromitite samples and several others from dunites with disseminated chromite, were investigated microscopically and microanalytically.

Electron microprobe analyses were performed using an ARL-SEMQ electron microprobe, operated in the WDS mode, at 15–25 kV accelerating voltage, and 15–20 nA beam current. Compositions of chromite and olivine were obtained from the analysis of several grains in each section. Quantitative determinations of Si, Ti, Al, Fe, Mn, Mg, Ca, Cr were calibrated on natural minerals: clinopyroxene, olivine, Mn-bearing hortonolite, chromite and ilmenite, whereas metallic Ni, V, and Zn were the standards for the corresponding elements. Trivalent iron in chromite was calculated assuming stoichiometry.

The PGMs were analyzed, using pure metals as the reference material for PGEs, and natural pyrite, niccolite, chalcopyrite, and stibine for Fe, Ni, Cu, S, As and Sb.

Total PGEs and Au were determined by ICP-MS at the University of Granada (Spain), after the Ni-sulfide-button preconcentration step, carried out at the University of Modena (Italy). The chromitite samples were powdered in an agate mill, and nickel sulfide (stoichiometry Ni_3S_2) beads of about 4 g were obtained by alkaline fusion at 1,000 °C of 10-g sample aliquots. Beads were dissolved in hot, concentrated HCl, then PGEs and Au were co-precipitated with metallic Te by adding stannous chloride to the solution. The insoluble precipitate was collected on filter paper, then washed to eliminate Ni, and dissolved in warm aqua regia. Spectrometric analysis was performed on the obtained solution after appropriate dilution, and calibrated using the UMT-1 standard certified by CANMET as the reference material. Limits of detection were 0.1 ppb for Ru, 0.05 ppb for Os, Rh, Pt and Pd, and 0.01 for Ir and Au.

Chromite mineralization in the Uktus complex

Field relationships and texture of chromite

Accessory chromite is ubiquitous in the dunites of the Uktus complex, occurring as euhedral to anhedral crystals from a few tens of microns up to more than 1 mm in size. Locally, chromite forms small, massive segregations of chromitite irregularly distributed through the dunites. Chromitites appear as tiny aggregates of a few millimeters, or consist of larger podiform veins and schlieren about 0.5–3 cm thick and 15–30 cm long. More extensive lenses and layers (up to some meters in size) are extremely rare and apparently restricted to the southern dunite body. Fourteen samples of chromitite and six of dunite with disseminated chromite were examined in this study, taken from surface outcrops and boreholes in the southern and northern dunite bodies (Fig. 1C).

The texture of accessory chromite is consistent with magmatic crystallization in equilibrium with the adjacent olivine. The small segregations, including veinlets and pods, usually consist of a central core of polygonal, closely packed chromite crystals, surrounded by symmetric rims of disseminated ore which fade out, grading without interruption into the accessory chromite in massive dunite. Some schlieren and layers display textures which are reminiscent of gravitational settling and cumulus formation of chromite crystals. They are typically asymmetric with a lower zone of polygonal, massive chromitite (< 10 vol% interstitial silicates) in sharp contact with underlying dunite, and grade upwards into middle- and low-grade disseminated chromite (40 to 60 vol% silicate). The transition from massive to disseminated ore is usually accompanied by a gradual decrease in size of the chromite grain. These textural features support the conclusion that chromitites in the Uktus complex formed during crystallization of their dunite host, possibly by accumulation of chromite grains, followed by slow cooling, annealing and sintering. Chromite is generally fresh, alteration being limited to development of ferrian chromite along grain boundaries and cracks. Fracturing of chromite occurred at some late stage, as testified by the secondary nature of the silicate filling of cracks and fissures, mainly consisting of chlorite, serpentine, and minor talc and carbonates.

Composition of chromite

Chromite covers a wide range of compositions in both massive and disseminated ore (Table 1, Fig. 2). The accessory chromite is invariably shifted towards higher $Fe^{2+}/(Fe^{2+}+Mg)$ with respect to massive segregations, which is interpreted as an effect of the subsolidus re-equilibration of the Fe^{2+}/Mg distribution between chromite and olivine at olivine/chromite mass ratios tending to infinity (Irvine 1967; Roeder 1994). In the ternary diagram Cr–Al–Fe^{3+}, the increase in Fe^{3+} occurs at the expense of Cr, whereas Al remains confined in the range 0.17–0.30 $Al/(Fe^{3+}+Cr+Al$; Fig. 3). The titanium content varies from 0.38 to 2.2 wt% TiO_2, showing negative correlation with Cr_2O_3 and positive correlation with Fe_2O_3 (Fig. 4). There is also a positive correlation of MnO (0.05–0.8 wt%), ZnO (0.12–0.65 wt%), and V_2O_3 (0.22–1.22 wt%) with $Fe^{2+}/(Fe^{2+}+Mg)$; NiO is usually lower than 0.20 wt%.

The iron enrichment in the Uktus chromites is striking. Relationships with the forsterite content of coexisting olivine (Fig. 5) indicate that the ratios $Fe^{2+}/(Fe^{2+}+Mg)$, $Fe^{3+}/(Fe^{3+}+Cr+Al)$ and $Fe^{3+}/(Fe^{3+}+Fe^{2+})$ increase in chromite from the southern to the northern dunite body, and from core to rim in single dunite bodies, as an effect of differentiation. Iron enrichment reaches its maximum in chromite from the marginal zone of the northern dunite. Here an unusual type of Cr-poor, Fe-rich chromitite was observed, consisting of a lamellar intergrowth between Ti-rich chromian magnetite and "picotite", in which minor geikielite occurs as part of the exsolution assemblage (Fig. 6). The bulk spinel phase has Cr_2O_3 as low as 20%, total FeO > 50%, Fe_2O_3 > 30%, and high TiO_2 contents (1.34–1.65 wt%). This composi-

Table 1 Selected microprobe analyses of chromite fromthe Uktus complex (*n.a.* not analyzed)

	SiO_2	TiO_2	Al_2O_3	FeO	Fe_2O_3	MgO	MnO	Cr_2O_3	NiO	ZnO	V_2O_3	Total
Massive												
410/37[a]	0.00	0.56	10.07	16.57	8.49	10.55	0.38	50.99	0.12	0.23	0.13	98.09
412/36[a]	0.01	0.58	11.84	15.64	9.24	12.23	0.29	51.52	0.23	0.02	0.11	101.71
UK272d[a]	0.15	0.53	12.36	15.31	6.19	12.05	0.24	51.61	0.12	0.10	0.10	98.76
UK273a[a]	0.04	0.74	13.42	18.52	10.18	10.35	0.34	46.53	0.15	0.07	0.17	100.51
UK274b[a]	0.05	0.75	12.59	17.53	10.79	10.49	0.25	45.35	0.14	0.12	0.17	98.23
UK277c[a]	0.03	0.38	14.93	12.57	4.52	13.99	0.28	52.26	0.11	0.12	0.05	99.24
UK296b[a]	0.08	0.72	12.00	17.14	14.64	11.32	0.31	44.82	0.11	0.03	0.13	101.30
UK298[a]	0.05	0.75	11.40	18.27	13.64	10.24	0.34	45.18	0.10	0.10	0.13	100.20
UK3	0.02	0.88	12.70	18.05	12.41	10.76	0.39	45.61	0.15	0.04	0.18	101.19
UK5	0.03	0.99	10.58	20.03	15.90	8.94	0.39	42.23	0.13	0.04	0.22	99.48
UK6	0.05	0.91	10.70	18.69	15.31	9.78	0.09	42.50	0.07	0.08	0.21	98.39
UK221	0.02	0.96	11.20	17.71	15.27	10.76	0.11	43.48	0.07	0.10	0.19	99.87
UK222av	0.10	1.40	12.13	21.41	33.83	8.00	0.20	19.88	0.15	0.12	0.48	97.70
UK222Al	0.03	0.40	35.43	14.27	12.46	14.87	0.24	21.07	0.12	0.31	0.22	99.42
UK222Fe	0.03	2.22	5.11	25.54	42.90	5.06	0.28	16.94	0.22	0.16	0.53	98.99
Disseminated												
410/37[a]	0.00	0.56	11.11	19.25	9.20	9.60	0.35	50.40	0.00	0.16	0.11	100.74
411/54[a]	0.00	0.52	11.77	19.13	10.74	9.68	0.35	48.44	0.12	0.11	0.00	100.86
412/36[a]	0.06	0.57	11.40	20.84	10.05	8.91	0.44	50.13	0.28	0.05	0.14	102.87
416/31[a]	0.05	0.75	11.43	22.67	16.21	7.12	0.54	40.93	0.12	0.23	0.15	100.20
438/50[a]	0.04	0.53	11.02	24.62	21.25	5.36	0.69	35.43	0.10	0.23	0.15	99.42
UK67[a]	0.00	0.67	12.97	22.64	11.86	8.02	0.42	45.12	0.10	n.a.	n.a.	101.80
UK70[a]	0.00	0.57	12.48	20.28	10.96	9.17	0.39	47.35	0.12	n.a.	n.a.	101.32
UK74[a]	0.00	0.52	11.92	18.94	8.30	9.65	0.33	50.92	0.12	n.a.	n.a.	100.70
UK1	0.07	0.98	7.74	24.47	23.73	5.42	0.45	35.09	0.09	0.07	0.23	98.34
UK2	0.04	0.97	10.97	23.32	18.66	6.78	0.47	38.13	0.10	0.09	0.21	99.74
UK4	0.05	0.71	12.61	21.32	12.17	7.83	0.50	42.89	0.19	0.17	0.16	98.60
UK33	0.00	1.31	15.86	22.01	18.46	8.76	0.45	33.42	n.a.	n.a.	n.a.	100.27
UK221	0.15	0.89	10.85	19.87	13.87	8.94	0.29	43.12	0.09	0.15	0.23	98.45
UK193	0.00	1.04	11.09	22.77	18.53	7.22	0.55	38.66	0.09	n.a.	n.a.	99.95
UK202	0.00	1.94	16.65	25.17	27.84	6.43	0.72	20.94	0.28	n.a.	n.a.	99.97

[a]Southern dunite body

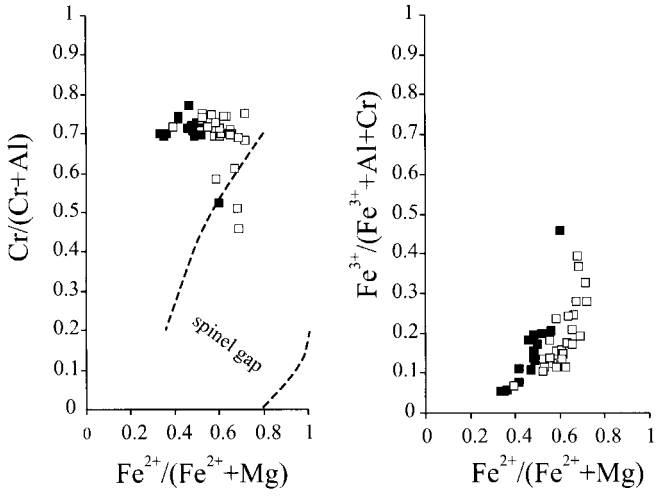

Fig. 2 Compositional variations of chromite from the Uktus complex. *Closed squares* Massive chromitite, *open squares* accessory chromite in dunite. Note the shifting of accessory chromite towards higher $Fe^{2+}/(Fe^{2+}+Mg)$ ratios, possibly as a result of subsolidus equilibration with large volumes of olivine (Irvine 1967). The most Cr-poor and Fe-rich chromitite plotting in the "spinel gap" (Roeder 1994) corresponds to the bulk composition (Table 1, anal. UK222av) of the exsolution intergrowth shown in Fig. 6, consisting of "picotite" (Table 1, anal. UK222Al) and chromian–titanomagnetite (Table 1, anal. UK222Fe)

tion plots in the Fe-rich and Cr-poor field (Fig. 2), within the "spinel miscibility gap" (Roeder 1994), indicating that the magnetite–picotite intergrowth probably resulted

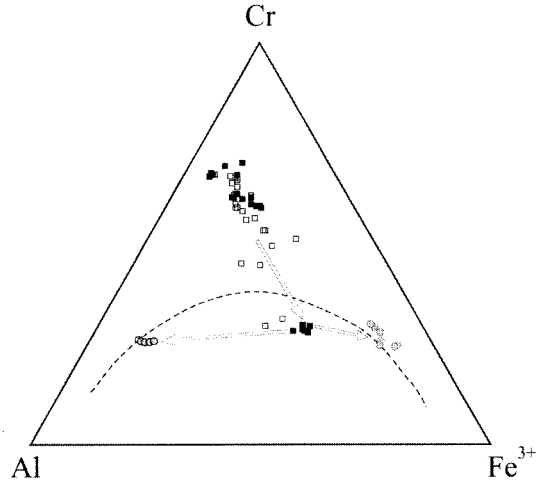

Fig. 3 Cr–Al–Fe^{3+} diagram of Uktus chromite samples. The *arrow* indicates the trend of Fe^{3+} enrichment with differentiation. The *dashed line* approximately represents the position of the miscibility gap for natural spinels (Roeder 1994). The most Fe-rich chromitite in Uktus (Table 1, sample UK222av) decomposes into "picotite" (Table 1, anal. UK222Al) and chromian–titanomagnetite (Table 1, anal. UK222Fe) (*shaded circles*; other symbols as in Fig. 2)

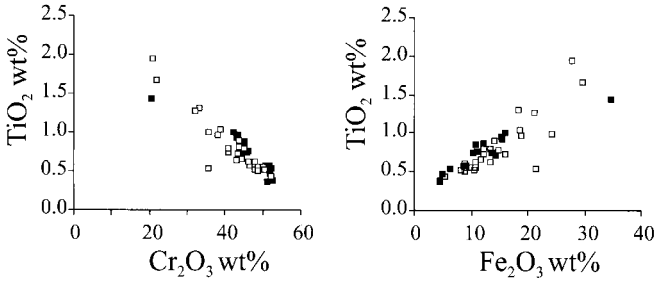

Fig. 4 TiO_2 content in chromite versus Cr_2O_3 and Fe_2O_3 (symbols as in Fig. 2)

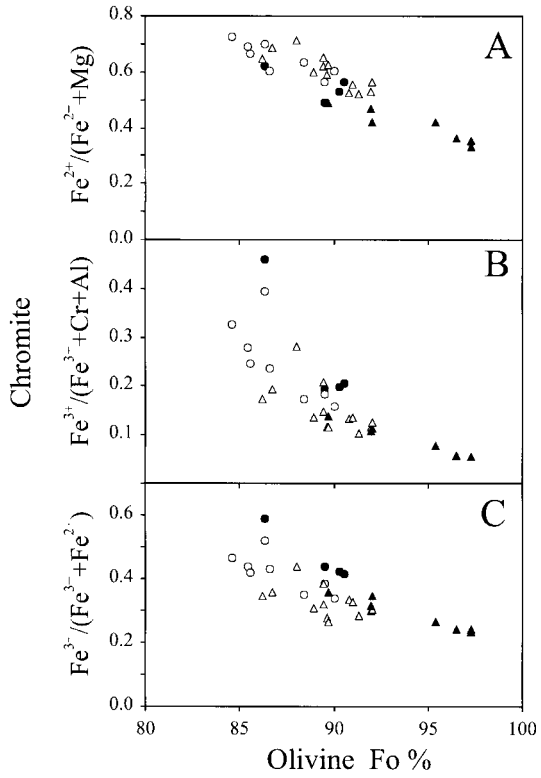

Fig. 5A–C Trends of Fe^{2+} and Fe^{3+} enrichment in Uktus chromite samples as a function of the decrease of the forsterite content (Fo%) in coexisting olivine. *Triangles* Southern dunite, *circles* northern dunite, *closed symbols* massive chromite, *open symbols* accessory chromite in dunite

from decomposition of the spinel on cooling. In the ternary diagram Cr–Al–Fe^{3+} (Fig. 3), the compositions of the exsolved spinels fit the chromite solvus line at about 800 °C (Pushkarev et al. 1999).

Temperature and oxygen fugacity

Results obtained from the olivine–spinel Fe^{2+}–Mg exchange thermobarometer (Ballhaus et al. 1991) are strongly affected by variations in chromite/olivine mass ratio and, possibly, the rate of cooling (Table 2). In

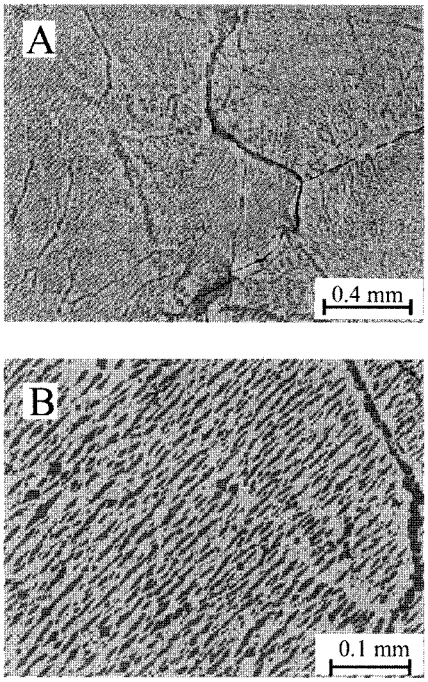

Fig. 6A, B BSE images of the exsolution intergrowth consisting of Al-rich spinel ("picotite") and chromian–titanomagnetite from the northern Fe-enriched dunite body (analyses: UK222Al and UK222Fe, Table 1). Composition of the bulk phase (anal. UK222av, Table 1) was obtained by scanning microprobe analysis with a large-spot electron beam of about 100 mμ. **A** Large field image of several chromite grains. **B** Unmixing texture in a single grain

general, massive chromite equilibrated at higher temperature and oxygen fugacity than the accessory chromite, and the highest values are observed in chromitites from the marginal zone of the northern dunite body, possibly as a result of more rapid cooling compared with chromitites from the core of the large dunite body. Oxygen fugacities calculated from the Uktus samples decrease with temperature along a T–fO_2 trend roughly parallel to the FMQ reaction line (Fig. 7A), and they fit the field of Uralian-Alaskan-type complexes at an oxidation state of 3–6 log units higher than ophiolitic chromites from the Urals (Chashchukhin et al. 1998).

The oxidation ratio $Fe^{3+}/(Fe^{3+}+Fe^{2+})$ in the Uktus chromites bears rough positive correlation with fO_2 not corrected for the temperature of subsolidus equilibration (Fig. 7B). The degree of correlation is very low in the accessory chromite ($r=0.54$) but increases significantly ($r=0.81$) in the massive chromite, suggesting that the variation in $Fe^{3+}/(Fe^{3+}+Fe^{2+})$ probably reflects the original magmatic composition of chromite, unaffected by subsolidus equilibration with olivine. Since the oxidation ratio of chromite is extremely sensible to fO_2 (Hill and Roeder 1974), the trends defined by massive chromite in Figs. 5C and 7B may be taken as an indication that oxygen fugacity was increasing during fractionation of dunite and chromitite at Uktus.

Table 2 Temperature and oxygen fugacity (Ballhaus et al. 1991) for chromite–olivinepairs from Uktus

Sample	Chromite			Olivine		
	$Fe^{2+}/(Fe^{2+}+Mg)$	$Fe^{3+}/(Fe^{3+}+Fe^{2+})$	$Al/(Al+Cr+Fe^{3+})$	Fo (%)	T (°C)	$logfO_2$
Southern body						
Chromitite						
UK277b	0.33	0.24	0.28	95	982	−6.9
UK277c	0.35	0.23	0.29	95	937	−7.6
UK277 1	0.36	0.24	0.28	92	1,110	−5.9
UK274b	0.48	0.35	0.25	90	1,154	−5.1
UK272d	0.41	0.26	0.24	92	1,065	−6.3
412/36	0.41	0.34	0.22	92	1,169	−4.5
410/37	0.46	0.31	0.20	92	1,063	−6.0
Dunite						
UK51	0.69	0.35	0.25	87	881	−9.4
UK60	0.65	0.34	0.25	86	944	−8.5
UK67	0.61	0.32	0.25	89	899	−8.9
UK69	0.62	0.26	0.22	90	850	−10.1
UK70	0.55	0.32	0.24	91	945	−7.8
UK74	0.52	0.28	0.23	91	947	−8.0
UK76	0.60	0.30	0.24	89	918	−8.8
UK80	0.58	0.27	0.23	89	907	−9.1
438/50	0.72	0.43	0.22	88	876	−8.9
416/31	0.65	0.38	0.22	89	910	−8.4
412/36	0.56	0.30	0.22	92	886	−8.8
411/54	0.52	0.33	0.23	91	1,019	−6.7
410/37	0.52	0.30	0.21	92	940	−7.9
Northern body						
Chromitite						
UK222 av	0.60	0.59	0.25	86	1,190	−4.2
UK221	0.48	0.43	0.22	89	1,276	−3.41
UK6	0.51	0.42	0.21	90	1,151	−4.66
UK5	0.55	0.41	0.21	91	1,067	−5.68
Dunite						
UK1	0.71	0.46	0.16	85	1,031	−6.84
UK2	0.65	0.41	0.22	86	1,038	−6.82
UK4	0.60	0.33	0.25	90	912	−8.47
UK221	0.55	0.38	0.22	89	1,079	−5.88
UK222	0.68	0.51	0.29	86	973	−7.22
UK33	0.58	0.43	0.31	87	1,078	−6.08
UK34	0.67	0.43	0.28	85	976	−7.62
UK35	0.63	0.34	0.21	88	955	−8.02

The PGE mineralization in the Uktus chromitites

Results of the PGE analysis for three chromitites from Uktus are compared with background concentrations in dunite, clinopyroxenite and gabbros (Table 3) and plotted as spider diagrams after normalization to the primitive mantle in Fig. 8. The chromitites display three distinctive types of PGE patterns corresponding to three different PGM assemblages (Table 4), which conspicuously correlate with changes in chromite composition (Fig. 9).

The type I PGE distribution pattern has a negative slope, with Os, Ir, and Ru predominating over Pt, Rh, and Pd, and it is found in chromitites from the southern dunite body, consisting of magnesiochromite with low $Fe^{3+}/(Fe^{3+}+Fe^{2+})=0.23$–$0.35$ and Mg-rich olivine (Fo = 90–96%). In agreement with the PGE distribution, the PGM assemblage consists of primary laurite, kashinite and cuproiridsite, whereas Pt and Pd PGM are absent. Irarsite and tolovkite are secondary minerals formed as a result of PGE remobilization at relatively low temperature. The primary Ir sulfides usually form composite inclusions with undefined Ni-Fe-rich Ir sulfide (Fig. 10A). Microprobe analyses (Table 5) show that laurite compositions vary from $Ru_{86}Os_7Ir_7$ to $Ru_{64}Os_{26}Ir_{10}$ (cf. Fig. 11).

The type II PGE distribution pattern, characterized by an M-like shape with marked peaks of Pt and Ir and $Pt_N/Ir_N > 1$, is found in magnesiochromitite from both the southern and northern dunite, with oxidation ratios $Fe^{3+}/(Fe^{3+}+Fe^{2+})=0.40$–$0.44$ and Mg-rich olivine (Fo = 88–92%). Consistent with the PGE analysis, the PGM assemblage is characterized by the predominance of primary Pt–Fe alloys and Ir–PGMs, and the absence of Ru and Pd phases. A number of secondary PGMs are found as replacement of the primary ones (tulameenite, unknown Rh_4S_3, potarite and one unidentified Ir–Fe oxide) or in close association with ferrian chromite, serpentine and chlorite (geversite). The Pt–Fe alloys (Table 6) contain less than 3 atom% Ni + Cu, and range between $Pt_{3.22}Fe_{0.78}$ and $Pt_{2.44}Fe_{1.56}$ with an average of $Pt_{2.95}Fe_{1.05}$, very close to the ideal Pt_3Fe stoichiometry characteristic of isoferroplatinum (Fig. 12). In the southern dunite body, Pt_3Fe forms composite grains

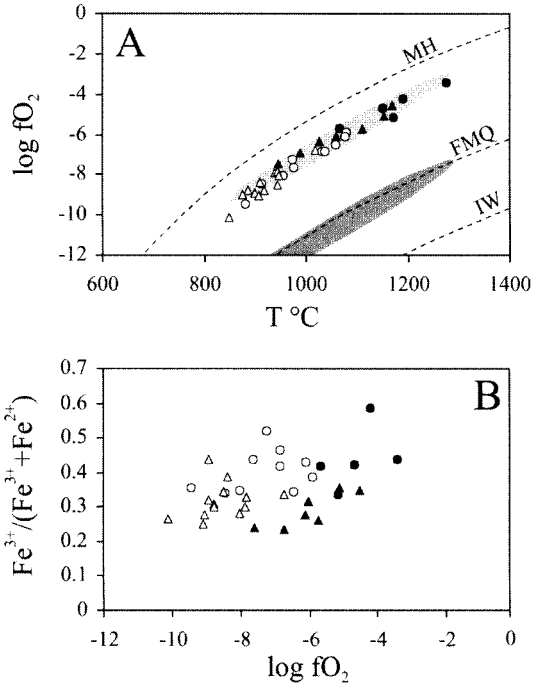

Fig. 7 **A** Calculated oxygen fugacity for chromite–olivine pairs from Uktus. *Lightly shaded field* Alaskan-type complexes, *darkly shaded field* dunite, harzburgite and chromitite from ophiolites of the Urals (data from Chashchukin et al. 1998, Pushkarev 2000). Variations of the MH, FMQ, and IW buffers with temperature are according to Ballhaus et al. (1991). **B** Variation of the oxidation ratio $Fe^{3+}/(Fe^{3+}+Fe^{2+})$ in massive and accessory chromite as a function of oxygen fugacity (not corrected for temperature). Symbols are as in Fig. 5

with erlichmanite, cuproiridsite and cuprorhodsite (Fig. 10B–E), coexisting with free grains of malanite and cooperite (Table 7). In the northern dunite body, the Pt_3Fe is enriched in Ir compared with Pt_3Fe from the southern body (Table 6, anal. 221 1a, b) and, significantly, is associated with Os-rich iridium (Table 7), in the apparent absence of any PGM sulfide.

The type III PGE distribution pattern is found in the Fe-rich chromitite ($Fe^{3+}/(Fe^{3+}+Fe^{2+})=0.59$) in Fe-rich dunite (Fo = 85%) from the northern body. It is characterized by an M-like shape similar to type II, although having Pt_N/Ir_N lower than unity, and relatively higher Pd and Rh. The PGM assemblage consists of irarsite, tulameenite, Rh–Sb–S compound, Pt–Pd–Cu, and Pd–Cu alloys along with Pd-rich copper all occurring as irregular grains, laths or specks inside picotite (Fig. 10F). Only irarsite could be quantitatively analyzed. However, the alloys and antimonides are compositionally similar to secondary PGMs observed in several samples (Table 8). Therefore, it is difficult to establish whether the PGMs of type III are primary magmatic or formed at some stage during subsolidus equilibration of the spinel host. Because of this uncertainty, the role of type III PGMs as indicators of high-T magmatic conditions remains questionable.

Estimated conditions of sulfur fugacity

The variations in PGM assemblage from one chromitite type to the other can be understood in terms of PGE alloy–sulfide equilibrium, as a function of fS_2 and temperature (Stockman and Hlava 1984). The composition of laurite in the type I assemblage remains confined between the Ru/Os atomic ratios of 13.3 and 2.5 (Fig. 11), therefore indicating a maximum crystallization temperature close to 1,300 °C at a sulfur fugacity of log $fS_2 = -1.3$, for the near-end-member laurite (Brenan and Andrews 2001). Such conditions are comparable with those prevailing in most chromitites from the ophiolitic mantle in which laurite is expected to coexist with Os–Ir alloys (Augé and Johan 1988; Garuti et al. 1999). The appearance of Ir and Rh sulfides would indicate an increment in fS_2 of about one log unit, up to the stability field of Ir_2S_3 (kashinite). The type II assemblage is consistent with the theoretical prediction that the Pt-rich phase Pt_3Fe isoferroplatinum may crystallize in equilibrium with cooperite, kashinite and Ir thiospinels (Skinner et al. 1976; Makovicky and Karup-Møller 2000). The presence of erlichmanite in the association suggests that sulfur fugacity reached the Os–OsS_2 reaction line, corresponding to log $fS_2 = -1$ at 1,100 °C. Precipitation of Pt_3Fe continued under decreasing fS_2, leading to the formation of a PGM assemblage dominated by Pt–Ir alloys. In the northern dunite body, Pd and Rh become important constituents of the assemblage. Their association with As and Sb may not be a secondary feature, but possibly indicates an increase in the activity of these volatiles (but not S) in the late stages of dunite fractionation at Uktus. In general, the primary

Table 3 Platinum-group element and gold concentrations(ppb) in rocks of the Uktus complex

Sample	Rock	Os	Ir	Ru	Rh	Pt	Pd	Au
UK277	Chromitite	101	503	154	13	48	2.1	1.1
UK6	Chromitite	23	109	9.6	15	1,050	7.4	219
UK222	Chromitite	93	441	19	55	428	32	6.8
UK1	Dunite	1.0	6.5	6.6	1.1	70	3.7	16
UK2	Dunite	5.7	8.8	11	2.6	163	16	32
UK4	Dunite	1.5	2.0	5.0	0.4	13	2.0	3.8
411/54	Dunite	5.9	8.7	6.8	1.5	20	6.8	5.1
UK7	Ol-gabbro	0.6	0.3	0.5	0.2	18	18	10
UK8	Gabbro	4.2	1.4	3.3	1.2	50	48	6.5
UK9	Pyroxenite	2.1	0.4	1.0	0.4	24	8.8	9.1

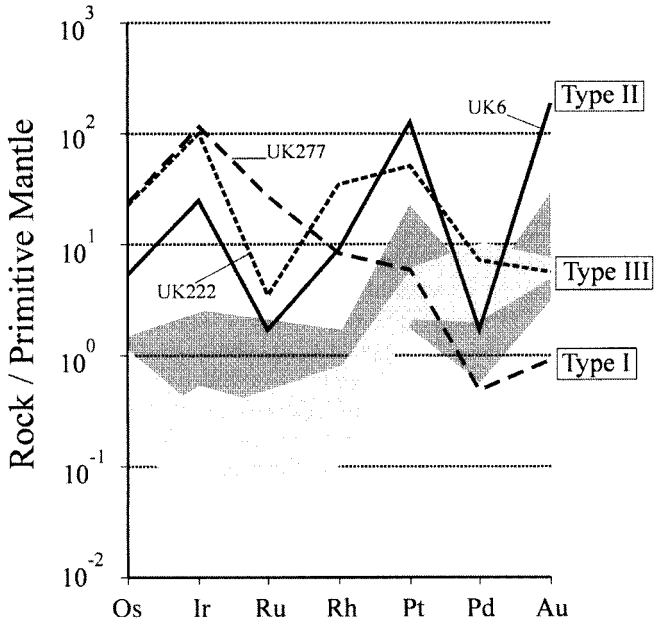

Fig. 8 Mantle-normalized PGE patterns for chromitites UK277, UK6, UK222 characterized by different types of PGM assemblage (see text for explanation). Compositional fields of dunites (*dark shading*) and clinopyroxenite–gabbro (*light shading*) are from Table 3 and Garuti et al. (1997a). Normalization values of primitive mantle are from Barnes et al. (1988)

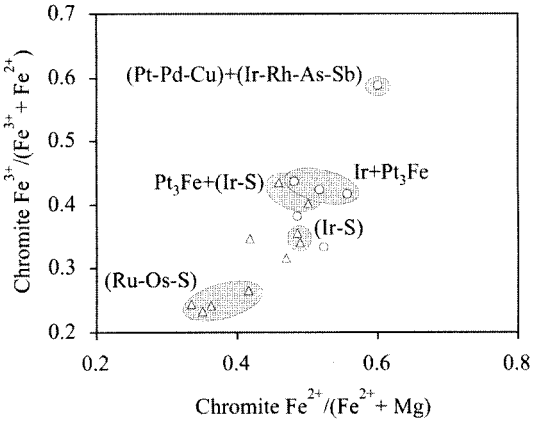

Fig. 9 Relationship between PGM assemblage and composition of the enclosing chromite in terms of oxidation ratio and ferrous-iron number. *Ru–Os–S* and *Ir–S* Type I assemblage in Table 4, *Pt_3Fe+(Ir–S)* and *Ir+Pt_3Fe* type II assemblage in Table 4, *(Pt–Pd–Cu)+(Ir–Rh–As–Sb)* type III assemblage in Table 4. *Triangles* Chromitite from the southern dunite body, *circles* chromitite from the northern dunite body

PGM assemblage associated with the Uktus chromitites indicates that the sulfur fugacity remained confined well below the values required for sulfur saturation of the melt and segregation of an immiscible sulfide liquid in the chromite-forming system.

Discussion

A major finding of this study is that the chromite-PGE mineralization of the Uktus Uralian-Alaskan-type complex originated at high magmatic temperature and underwent equilibration in a thermal range of 1,276–850 °C. The chromitites are syngenetic with their dunite host. Therefore, they have to be distinguished from certain Pt-rich chromitites reported from Nizhny Tagil which are believed to have an epigenetic relationship with the adjacent dunite (Betechtin 1961). The great bulk of the PGMs in the Uktus chromitites (Pt_3Fe, iridium, cooperite, malanite, kashinite, cuproiridsite, cuprorhodsite, erlichmanite, and laurite) are early magmatic phases included in chromite. Only a small part of the PGM assemblage (tulameenite, irarsite, tolovkite, geversite, potarite and other unidentified Pt–Pd–Cu and Pd–Cu alloys) display features of late minerals formed at some post-magmatic stage as a result of PGE remobilization during hydrothermal or metamorphic episodes.

The PGE fractionation in the chromitites started with Ru, Os, and Ir but moved soon to selective precipitation of Pt and Ir, giving rise to the M-shaped PGE patterns similar to those in other Uralian-Alaskan-type chromitites (i.e., St. Louis et al. 1986; Nixon et al. 1990). The Pt anomaly is also reflected in the dunites of the Uktus complex which are enriched in Pt with respect to the primitive mantle. However, the Pt anomaly progressively attenuates in clinopyroxenite and gabbros, parallel to the differentiation trend (Garuti et al. 1997a). Apparently, the compatible behavior of Pt which precipitates with the refractory Ir does not obey the commonly observed order of PGE fractionation based on decreasing melting point and increasing solubility in silicate melts (Barnes et al. 1985), neither is it triggered by segregation of magmatic sulfides, as occurs in Pt-Pd-enriched chromitites from layered intrusions and ophiolite complexes (Naldrett and Von Gruenewaldt 1989).

Table 4 PGM assemblages in chromitites of the Uktus complex (number of grains in brackets)

	Primary PGMs	Secondary PGMs
Type I	(Ru–Os–S)+(Ir–S) Laurite(13), kashinite (3), cuproiridsite (1)	(Ir–As–Sb) Irarsite(2), tolovkite (1)
Type II	(Pt_3Fe+Ir–S)or (Ir+Pt_3Fe) Pt_3Fe(80), osmium (4), iridium (10) Erlichmanite(7), malanite (3), cuproiridsite (2) Cuprorhodsite(3), cooperite (2)	(Pt–Cu,Pt–Ir–Sb, Ir–O, Pd–Hg) Tulameenite(14), potarite (1) Geversite(1) Un.Rh4S3 (1), un. Ir–Fe oxide (1)
Type III	(Pt–Pd–Cu)+(Ir–Rh–As–Sb) Pt–Pd–Cu(4), Rh–Sb–S (1) Irarsite(2), tulameenite (1)	

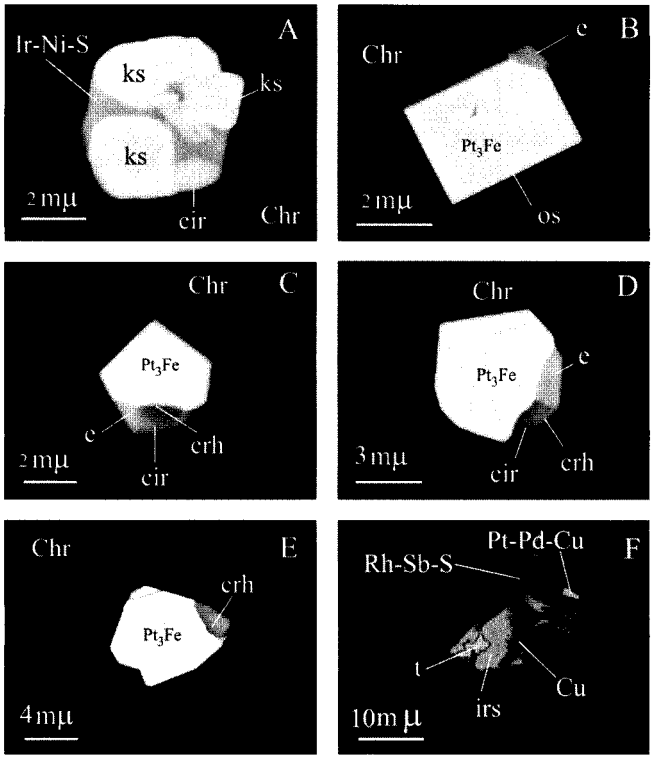

Fig. 10A–F BSE images of PGMs from the Uktus chromitites. **A)** Type I assemblage: composite grain of kashinite (*ks*), cuproiridsite (*cir*), and an unknown Ir–Ni–S sulfide included in chromite (*Chr*). **B–E** Type II assemblages: composite grains of Pt_3Fe (isoferroplatinum?) with osmium (*os*), erlichmanite (*e*), cuproiridsite (*cir*), and cuprorhodsite (*crh*) included in chromite. **F** Type III assemblage consisting of irarsite (*irs*) and tulameenite (*t*) associated with Pd-rich copper (*Cu*), Pt–Pd–Cu alloy and unidentified Rh–Sb–S associated with amphibole? (*dark shading*) and the "picotite" phase (*medium shading*) in unmixed Fe-rich chromite (sample UK222)

Clearly, this fact requires a sharp drop of Pt solubility in the mafic melt, and stabilization of abundant Pt–Fe alloys—two processes whose controlling factors have not been completely understood so far.

The role of oxygen fugacity, and iron activity

The case of Uktus provides the important indication that both total iron and oxidation ratio increased in chromite during fractional crystallization of the dunites. Furthermore, a sharp drop of Pt solubility, with extensive precipitation of Pt–Fe alloys, occurred in a very restricted range of conditions, corresponding to fractionation of magnesiochromite with high oxidation ratio (>0.4). Significantly, no crystallization of Pt phases occurred in magnesiochromite at low oxidation state (<0.3), suggesting that the metal remained in the silicate liquid whereas laurite and Ir sulfides were the only crystallizing PGMs.

Most experimentalists agree that under conditions below sulfur saturation, the solubility of Pt in silicate melts decreases with temperature and with increasing SiO_2 activity. There has been, however, considerable debate concerning the role of oxygen fugacity which was reported to have contrasting effects on the solubility of Pt (Amossé et al. 1990; Borisov and Palme 1997). If we accept the assumption that the oxidation ratio in the massive chromites of Uktus was increasing due to increase of fO_2 during fractionation, then the selective precipitation of Pt at relatively high oxidation ratios would seem to be consistent with the experiments indicating that the Pt solubility in basaltic melts has a negative correlation with oxygen fugacity (Amossé et al. 1990). However, in experiments with Fe-free silicate melts, the solubility of Pt was observed to increase with increasing oxygen fugacity (Borisov and Palme 1997) and, more recently, such a positive correlation was found to be valid even for Fe-bearing silicate melts (Borisov and Palme 2000). The reasons for such a discrepancy may be various and diverse (Amossé and Allibert 1993; Amossé et al. 2000). However, all experiments apparently agree on the conclusion that high iron activity in silicate melts has a very strong effect in enhancing the stability of Pt–Fe alloys, causing considerable reduction of the Pt solubility in magmas. This implies that precipitation of Pt in Fe-rich melts may occur independently from the true variation in oxygen fugacity, and may simply reflect an increase in FeO activity during fractionation.

This alternative mechanism is based on the observation that Uralian-Alaskan-type magmas are characterized by low silica activity, which favors initial stabilization of olivine instead of orthopyroxene and produces an increase in the Fe_2O_3 and Fe_3O_4 activity in the melt. Under these conditions, fractionation causes increasing amounts of magnetite to be incorporated in the coexisting chromite which becomes enriched in total iron and has a higher oxidation ratio compared with chromites commonly derived from tholeiitic and high-alumina basalts (Irvine 1967). The effect on chromite composition is the same as that of increasing the oxygen fugacity in the melt, although the intrinsic variation in oxygen fugacity during fractionation would have little influence, and co-precipitation of iron-rich chromite and Pt–Fe alloys may be a result of the critical undersaturation in silica of Uralian-Alaskan-type magmas.

The behavior of Ir and Ru

Most precipitation of Ir in the Uktus complex is limited to the chromitite event, which apparently depresses almost completely the Ir activity in the residual melt, as demonstrated by the sharp reduction of the Ir peak in dunites. The geochemical behavior of Ir in Uktus is therefore consistent with experimental observations indicating that Ir is remarkably less soluble than Pt in silicate melts (Amossé et al. 1990). The positive Ir anomaly in chromitites correlates with a negative anomaly in Ru. In fact, after an initial stage dominated

Table 5 Selected microprobe analyses of PGM sulfidesfrom type I assemblage

	Os	Ir	Ru	Rh	Pt	Pd	Ni	Fe	Cu	S	Total
Wt%											
272D 1	7.40	5.41	49.9	1.65	0.06	0.00	0.07	0.68	0.01	35.3	100.48
272D 2	8.12	5.46	47.5	2.16	0.00	0.00	0.04	0.74	0.00	35.6	99.62
272D 3	7.12	5.48	50.4	1.74	0.00	0.00	0.08	0.65	0.01	36.0	101.48
272D 4	7.46	5.18	51.6	1.44	0.18	0.00	0.06	0.8	0.00	35.9	102.62
277B 1 1	22.4	8.21	36.8	0.30	0.14	0.00	0.03	0.71	0.00	32.7	101.29
277B 1 2	23.2	7.91	34.8	0.60	0.00	0.00	0.01	0.62	0.00	31.9	99.04
277B 1 3	25.6	8.47	34.0	0.72	0.21	0.00	0.06	0.72	0.03	31.5	101.31
277C 11	15.6	6.49	40.9	0.92	0.00	0.00	0.05	0.63	0.03	34.8	99.42
277C 1	17.9	5.70	37.0	0.80	0.14	0.00	0.11	4.88	0.00	33.5	100.03
277C 1 2	14.9	6.92	41.1	0.82	0.00	0.11	0.06	0.68	0.04	34.4	99.03
277C 2	16.6	7.95	39.7	0.99	0.27	0.00	0.03	1.93	0.00	31.2	98.67
277C 3	17.4	9.88	38.2	0.93	0.14	0.00	0.02	1.83	0.00	30.4	98.80
277C 4	16.1	8.87	39.9	0.70	0.00	0.00	0.08	1.57	0.00	30.2	97.42
274B 1 1	1.54	52.4	0.30	18.4	0.28	0.00	0.37	1.40	0.18	22.9	97.77
274B 1 3	0.00	48.6	0.01	26.8	0.19	0.75	0.19	1.34	0.07	24.3	102.25
274B 1 6	0.32	34.5	0.01	10.1	0.43	0.00	14.5	6.43	3.84	25.2	95.33
Atomsper formula unit											
272D 1	0.07	0.05	0.88	0.03	0.00	0.00	0.00	0.02	0.00	1.95	3.00
272D 2	0.08	0.05	0.84	0.04	0.00	0.00	0.00	0.02	0.00	1.98	3.00
272D 3	0.07	0.05	0.87	0.03	0.00	0.00	0.00	0.02	0.00	1.96	3.00
272D 4	0.07	0.05	0.89	0.02	0.00	0.00	0.00	0.02	0.00	1.95	3.00
277B 1 1	0.23	0.08	0.70	0.01	0.00	0.00	0.00	0.02	0.00	1.96	3.00
277B 1 2	0.24	0.08	0.68	0.01	0.00	0.00	0.00	0.02	0.00	1.96	3.00
277B 1 3	0.27	0.09	0.66	0.01	0.00	0.00	0.00	0.03	0.00	1.94	3.00
277C 11	0.15	0.06	0.75	0.02	0.00	0.00	0.00	0.02	0.00	2.00	3.00
277C 1	0.17	0.05	0.67	0.01	0.00	0.00	0.00	0.16	0.00	1.92	3.00
277C 1 2	0.15	0.07	0.75	0.01	0.00	0.00	0.00	0.02	0.00	1.99	3.00
277C 2	0.17	0.08	0.76	0.02	0.00	0.00	0.00	0.07	0.00	1.89	3.00
277C 3	0.18	0.10	0.75	0.02	0.00	0.00	0.00	0.07	0.00	1.88	3.00
277C 4	0.17	0.09	0.79	0.01	0.00	0.00	0.00	0.06	0.00	1.88	3.00
274B 1 1	0.03	1.12	0.01	0.74	0.01	0.00	0.03	0.10	0.01	2.95	5.00
274B 1 3	0.00	0.97	0.00	1.00	0.00	0.03	0.01	0.09	0.00	2.90	5.00
274B 1 6	0.01	0.84	0.00	0.46	0.01	0.00	1.16	0.54	0.28	3.69	7.00

by laurite, Ru stops precipitating, although crystallization of Os and Ir sulfides continues. This feature may be explained either by a rapid decrease of Ru activity in the melt or by an increase in Ru solubility with increasing oxygen fugacity (Amossé and Allibert 1993; Amossé et al. 2000; Borisov and Palme 2000), or both.

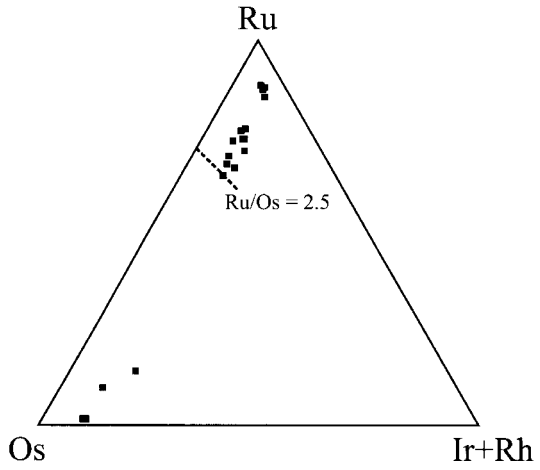

Fig. 11 Ru–Os–Ir (atom%) compositions of laurite in type I assemblage, and erlichmanite in type II assemblage

Origin of the Pt and Ir anomalies in Uralian-Alaskan-type magmas

The PGE data from the Uktus Uralian-Alaskan-type complex show that chromitites are characterized by strong positive anomalies of both Ir and Pt, and that the Pt anomaly, although low in absolute values, persists in dunite, wehrlite, olivine clinopyroxenite, and olivine gabbro of Uktus. Literature data show that the Pt anomaly is also present in hornblendite and hornblende–plagioclase pegmatite from a number of Uralian-Alaskan-type complexes (St. Louis et al. 1986; Tistl 1994; Garuti et al. 1997a), thus indicating that the chromitite–dunite event could not consume the Pt content of the magma completely. Unfortunately, we do not have knowledge of the initial concentration of Pt and Ir in the parent melt of the Uktus complex. However, the very high Ir content of chromitites and the persistence of a Pt anomaly in all rocks of Uktus appear not to be a simple effect of fractionation under particular conditions of oxygen fugacity and silica activity, but may represent a distinctive signature of Uralian-Alaskan-type magmas, possibly reflecting Pt–Ir enrichment in their mantle source (Garuti et al. 1997a).

The existence of such Pt-Ir-rich mantle in nature has been proposed based on the indirect evidence that

Table 6 Selected microprobe analyses of Pt–Fealloys from type II PGM assemblage

	Os	Ir	Ru	Rh	Pt	Pd	Ni	Fe	Cu	Tot.
Wt%										
298A 4b	0.00	2.31	0.01	1.04	88.1	0.06	0.18	8.85	0.26	100.81
298A 5	0.00	1.95	0.05	0.92	87.6	0.19	0.22	9.65	0.21	100.79
298A 7	0.01	2.10	0.11	1.39	88.3	0.09	0.32	8.95	0.27	101.54
298A 8	0.12	1.41	0.10	1.14	87.5	0.23	0.26	9.92	0.27	100.95
298A 9	0.19	1.72	0.04	0.92	87.5	0.25	0.30	9.92	0.24	101.08
298A 10	1.16	0.94	0.16	1.15	85.5	0.35	0.20	9.79	0.26	99.51
298B 2b	0.04	1.56	0.19	1.41	87.7	0.32	0.27	9.26	0.40	101.15
298B 3	0.00	0.37	0.00	1.08	87.3	0.48	0.27	10.0	0.27	99.77
298B 4	0.07	1.44	0.07	0.91	88.4	0.44	0.24	9.58	0.27	101.42
298B 7	0.20	1.49	0.07	1.19	86.4	0.33	0.26	9.30	0.27	99.51
298B 8	0.59	1.51	0.12	1.41	86.9	0.34	0.22	8.87	0.26	100.22
298B 9	0.17	1.52	0.05	1.25	85.8	0.33	0.34	9.75	0.30	99.51
298B 14	0.00	1.45	0.04	1.29	86.2	0.33	0.24	9.37	0.27	99.19
296A 5a	0.03	1.74	0.13	1.16	86.0	0.00	0.21	9.82	0.27	99.36
296A 8a	0.06	1.75	0.03	0.80	86.6	0.24	0.26	9.24	0.27	99.25
296A 8b	0.00	1.71	0.05	0.71	87.6	0.40	0.32	10.0	0.30	101.09
296A 10	0.11	1.45	0.09	1.37	85.9	0.31	0.25	9.47	0.27	99.22
296A 14	0.10	1.81	0.08	0.91	85.5	0.20	0.31	10.3	0.17	99.38
296B 1a	0.36	1.58	0.02	1.28	86.6	0.00	0.20	9.32	0.26	99.62
296B 7	0.31	0.24	0.00	1.01	85.6	0.26	0.27	10.2	0.26	98.15
296B 10	0.09	1.44	0.06	1.04	85.8	0.01	0.21	9.07	0.33	98.05
296B 16	0.10	0.89	0.00	0.77	85.6	0.13	0.31	10.4	0.32	98.52
296B 18	0.15	1.18	0.00	0.93	85.7	0.39	0.28	10.6	0.33	99.56
296B 21	0.10	1.44	0.08	0.88	86.0	0.21	0.22	9.77	0.23	98.93
221 1a	0.00	4.22	0.01	0.96	80.6	0.26	0.63	10.6	0.00	97.28
221 1b	0.00	4.55	0.00	1.85	79.1	0.00	0.53	12.2	0.00	98.23
Atoms per formula unit										
298A 4b	0.00	0.08	0.00	0.06	2.82	0.00	0.02	0.99	0.03	4.00
298A 5	0.00	0.06	0.00	0.05	2.76	0.01	0.02	1.06	0.02	4.00
298A 7	0.00	0.07	0.01	0.08	2.79	0.01	0.03	0.99	0.03	4.00
298A 8	0.00	0.04	0.01	0.07	2.73	0.01	0.03	1.08	0.03	4.00
298A 9	0.01	0.05	0.00	0.05	2.73	0.01	0.03	1.08	0.02	4.00
298A 10	0.04	0.03	0.01	0.07	2.70	0.02	0.02	1.08	0.03	4.00
298B 2b	0.00	0.05	0.01	0.08	2.75	0.02	0.03	1.02	0.04	4.00
298B 3	0.00	0.01	0.00	0.06	2.74	0.03	0.03	1.10	0.03	4.00
298B 4	0.00	0.05	0.00	0.05	2.77	0.03	0.02	1.05	0.03	4.00
298B 7	0.01	0.05	0.00	0.07	2.76	0.02	0.03	1.04	0.03	4.00
298B 8	0.02	0.05	0.01	0.09	2.78	0.02	0.02	0.99	0.03	4.00
298B 9	0.01	0.05	0.00	0.07	2.71	0.02	0.04	1.08	0.03	4.00
298B 14	0.00	0.05	0.00	0.08	2.75	0.02	0.03	1.05	0.03	4.00
296A 5a	0.00	0.06	0.01	0.07	2.73	0.00	0.02	1.09	0.03	4.00
296A 8a	0.00	0.06	0.00	0.05	2.78	0.01	0.03	1.04	0.03	4.00
296A 8b	0.00	0.05	0.00	0.04	2.73	0.02	0.03	1.09	0.03	4.00
296A 10	0.00	0.05	0.01	0.08	2.74	0.02	0.03	1.05	0.03	4.00
296A 14	0.00	0.06	0.00	0.05	2.69	0.01	0.03	1.13	0.02	4.00
296B 1a	0.01	0.05	0.00	0.08	2.77	0.00	0.02	1.04	0.03	4.00
296B 7	0.01	0.01	0.00	0.06	2.72	0.02	0.03	1.13	0.03	4.00
296B 10	0.00	0.05	0.00	0.06	2.79	0.00	0.02	1.03	0.03	4.00
296B 16	0.00	0.03	0.00	0.05	2.70	0.01	0.03	1.15	0.03	4.00
296B 18	0.00	0.04	0.00	0.05	2.67	0.02	0.03	1.15	0.03	4.00
296B 21	0.00	0.05	0.00	0.05	2.74	0.01	0.02	1.09	0.02	4.00
221 1a	0.00	0.14	0.00	0.06	2.55	0.02	0.07	1.17	0.00	4.00
221 1b	0.00	0.14	0.00	0.11	2.40	0.00	0.05	1.30	0.00	4.00

asthenosphere-derived melts bear significant negative anomalies of Pt and Ir, suggesting that these metals were retained in the mantle source (Garuti et al. 1997b). Moreover, the presence of Pt–Fe alloys has been documented in residual peridotites from orogenic mantle massifs (Garuti et al. 1984), demonstrating that Pt enrichment may have resulted from early accumulation of refractory alloys during partial melting. Late-stage re-melting of such residual mantle, possibly triggered by re-introduction of metasomatic fluids, may be at the origin of Pt- and Ir-rich Uralian-Alaskan-type magmas. The geodynamic setting of Uralian-Alaskan-type complexes of the Urals, coupled with an anomalous enrichment in incompatible trace elements in these ultramafic melts (Fershtater et al. 1998, 1999) suggest that fluid-driven mantle metasomatism in the subdudction zone of the Urals was a viable mechanism to produce re-melting of a depleted mantle, previously

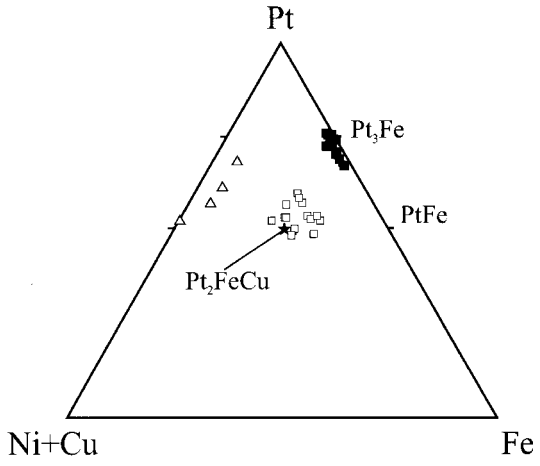

Fig. 12 Composition of Pt alloys plotted in the Pt–Fe–(Ni + Cu) ternary diagram (atom%). *Closed squares* Primary Pt–Fe alloys with isoferroplatinum-type stoichiometry (minor amounts of Ir and Rh have been added to Pt). *Open squares* Secondary Pt–Fe–Cu alloys with tulameenite-type stoichiometry (Cu > > Ni). *Triangles* Secondary Pt–Cu alloys containing about10–15 atom% Pd (Ni absent)

enriched in refractory Pt and Ir alloys by first-stage melting episodes.

Conclusions

The geochemical and mineralogical data of the Uktus chromitites presented in this study support the contention that high concentrations of Pt in Uralian-Alaskan-

Table 7 Selected microprobe analyses of PGM associatedwith Pt–Fe alloys in type II assemblage

	Os	Ir	Ru	Rh	Pt	Pd	Ni	Fe	Cu	S	Tot.
Wt%											
Southern dunite body											
296B 22	57.9	3.05	3.71	2.12	0.13	0.58	0.02	7.50	0.05	22.1	97.16
296B 23	48.4	5.58	4.95	2.73	5.21	0.27	0.00	10.6	0.00	21.9	99.64
298A 3 3	67.5	5.66	0.51	1.29	0.00	0.00	0.03	0.14	0.00	25.3	100.43
298A 3 9	68.5	4.51	0.51	1.58	0.00	0.07	0.02	0.13	0.00	24.6	99.92
296A 12	0.19	29.0	0.00	23.7	0.83	0.00	0.88	3.41	8.43	24.2	90.64
296A 3 1	0.00	17.4	0.00	12.2	33.5	0.00	0.04	1.40	10.8	24.1	99.44
296A 3 2	0.00	16.7	0.00	12.3	33.0	0.42	0.00	1.48	10.8	23.3	98.00
296A 4 1	0.07	19.5	0.00	10.1	32.8	0.00	0.11	2.07	10.2	23.1	97.95
298A 6 1	7.55	0.68	1.33	0.67	72.3	0.21	0.30	3.09	0.44	14.1	100.67
298B 5 2	0.04	0.26	0.00	0.61	84.9	0.36	0.46	1.25	0.00	13.0	100.88
Northern dunite body											
5 1a	12.3	73.2	1.79	2.24	5.98	0.00	0.07	1.77	0.00	0.17	97.52
5 1b	12.5	72.9	1.73	1.92	5.67	0.00	0.06	1.76	0.00	0.23	96.77
5 1c	12.9	72.5	1.84	1.91	5.80	0.04	0.03	2.10	0.00	0.04	97.16
6 1a	17.3	65.3	1.90	1.84	11.1	0.17	0.02	2.16	0.00	0.08	99.87
6 1b	17.6	66.5	1.86	2.34	10.3	0.00	0.09	2.22	0.00	0.03	100.94
6 1c	16.8	65.3	1.84	2.00	10.5	0.08	0.11	2.27	0.00	0.03	98.93
221b 1	22.8	66.5	1.69	1.32	5.95	0.05	0.00	0.73	0.00	0.05	99.09
221b 2	23.8	63.4	1.68	1.27	4.40	0.02	0.05	0.66	0.00	0.07	95.35
221b 3	24.0	62.1	1.84	1.19	4.63	0.00	0.00	1.14	0.02	0.15	95.07
221b 4	24.6	63.5	1.77	1.14	4.36	0.00	0.04	0.84	0.00	0.11	96.36
Atomsper formula unit											
Southern dunite body											
296B 22	0.76	0.04	0.09	0.05	0.00	0.01	0.00	0.33	0.00	1.71	3.00
296B 23	0.61	0.07	0.12	0.06	0.06	0.01	0.00	0.45	0.00	1.62	3.00
298A 3 3	0.89	0.07	0.01	0.03	0.00	0.00	0.00	0.01	0.00	1.98	3.00
298A 3 9	0.92	0.06	0.01	0.04	0.00	0.00	0.00	0.01	0.00	1.96	3.00
296A 12	0.01	0.78	0.00	1.19	0.02	0.00	0.08	0.32	0.69	3.91	7.00
296A 3 1	0.00	0.48	0.00	0.62	0.91	0.00	0.00	0.13	0.90	3.96	7.00
296A 3 2	0.00	0.47	0.00	0.64	0.91	0.02	0.00	0.14	0.91	3.90	7.00
296A 4 1	0.00	0.55	0.00	0.53	0.91	0.00	0.01	0.20	0.87	3.92	7.00
298A 6 1	0.08	0.01	0.03	0.01	0.79	0.00	0.01	0.12	0.01	0.93	2.00
298B 5 2	0.00	0.00	0.00	0.01	0.99	0.01	0.02	0.05	0.00	0.92	2.00
Northern dunite body											
5 1a	0.12	0.69	0.03	0.04	0.06	0.00	0.00	0.06	0.00	0.01	1.00
5 1b	0.12	0.69	0.03	0.03	0.05	0.00	0.00	0.06	0.00	0.01	1.00
5 1c	0.12	0.68	0.03	0.03	0.05	0.00	0.00	0.07	0.00	0.00	1.00
6 1a	0.16	0.60	0.03	0.03	0.10	0.00	0.00	0.07	0.00	0.00	1.00
6 1b	0.16	0.60	0.03	0.04	0.09	0.00	0.00	0.07	0.00	0.00	1.00
6 1c	0.16	0.60	0.03	0.03	0.10	0.00	0.00	0.07	0.00	0.00	1.00
221b 1	0.22	0.64	0.03	0.02	0.06	0.00	0.00	0.02	0.00	0.00	1.00
221b 2	0.24	0.63	0.03	0.02	0.04	0.00	0.00	0.02	0.00	0.00	1.00
221b 3	0.24	0.61	0.03	0.02	0.04	0.00	0.00	0.04	0.00	0.01	1.00
221b 4	0.24	0.62	0.03	0.02	0.04	0.00	0.00	0.03	0.00	0.01	1.00

Table 8 Selected microprobe analyses of PGM from type III and secondary assemblages (*n.a.* not analyzed)

	Os	Ir	Ru	Rh	Pt	Pd	Ni	Fe	Cu	S	As	Sb	Total
Wt%													
Type III PGM assemblage													
222 2 1	0.06	56.40	0.22	4.06	0.00	0.00	0.03	1.43	0.46	10.79	23.55	n.a.	97.01
222 2 2	0.00	58.40	0.32	3.16	0.41	0.00	0.05	1.48	0.64	11.37	22.08	n.a.	97.90
222 2 5	0.11	58.74	0.35	3.37	0.32	0.00	0.01	1.37	2.14	10.70	23.52	n.a.	100.64
Secondary PGMs													
273A 1 2	0.11	58.50	1.02	3.04	0.00	0.04	0.01	0.43	0.02	11.07	24.94	n.a.	99.19
273A 1 3	0.00	60.39	0.52	3.21	0.00	0.00	0.03	0.45	0.00	10.63	26.57	n.a.	101.80
416/32	0.08	0.00	0.06	0.23	41.37	0.00	0.63	0.38	0.00	0.00	1.49	55.01	99.24
296A 15 2	0.00	17.90	0.28	8.46	33.51	0.11	0.74	19.73	0.71	0.00	0.14	18.99	100.57
296A 15 4	0.08	17.49	0.00	7.79	32.27	0.51	0.67	19.95	0.71	0.00	0.02	19.87	99.35
273A 1 5	0.00	32.57	2.48	0.23	9.21	0.00	1.04	4.36	0.00	3.03	1.32	45.00	99.23
273A 1 6	0.13	32.51	3.18	0.13	11.07	0.00	1.11	4.45	0.01	2.94	1.53	44.02	101.07
296 6 1	0.11	1.56	0.09	0.77	75.47	0.00	0.83	12.26	6.64	n.a.	n.a.	n.a.	97.74
296A 9 2	0.00	0.38	0.06	0.15	73.80	0.06	1.44	12.22	9.27	n.a.	n.a.	n.a.	97.38
296B 17	0.00	0.50	0.10	0.66	76.02	0.11	1.29	14.70	5.92	n.a.	n.a.	n.a.	99.30
296B 9 3	0.00	1.97	0.08	0.94	75.81	0.00	2.05	11.06	7.29	n.a.	n.a.	n.a.	99.21
298 1 1	0.00	0.98	0.05	0.33	70.55	8.19	4.26	10.92	3.68	n.a.	n.a.	n.a.	98.96
298 1 2	0.00	0.66	0.00	0.20	77.82	0.39	5.10	12.32	3.79	n.a.	n.a.	n.a.	100.27
298 1 3	0.00	0.79	0.00	0.32	76.63	0.01	5.04	12.53	2.88	n.a.	n.a.	n.a.	98.21
298 1 4	0.28	0.75	0.00	0.20	76.81	0.13	4.41	13.42	3.38	n.a.	n.a.	n.a.	99.37
298A 3 1	0.00	1.02	0.00	0.44	77.10	0.01	0.33	9.66	12.64	n.a.	n.a.	n.a.	101.19
298A 3 4	0.00	0.38	0.05	0.38	78.61	0.34	1.70	13.73	5.71	n.a.	n.a.	n.a.	100.89
298A 3c	0.21	0.77	0.00	0.73	77.04	0.00	0.35	10.72	10.66	n.a.	n.a.	n.a.	100.48
298B 14a	0.17	0.23	0.00	0.24	77.17	0.00	1.86	11.49	9.07	n.a.	n.a.	n.a.	100.22
Atomsper formula unit													
Type III PGM assemblage													
222 2 1	0.00	0.86	0.01	0.12	0.00	0.00	0.00	0.08	0.02	0.99	0.92	0.00	3.00
222 2 2	0.00	0.89	0.01	0.09	0.01	0.00	0.00	0.08	0.03	1.04	0.86	0.00	3.00
222 2 5	0.00	0.87	0.01	0.09	0.00	0.00	0.00	0.07	0.10	0.95	0.90	0.00	3.00
Secondary PGMs													
273A 1 2	0.00	0.89	0.03	0.09	0.00	0.00	0.00	0.02	0.00	1.00	0.97	0.00	3.00
273A 1 3	0.00	0.90	0.01	0.09	0.00	0.00	0.00	0.02	0.00	0.95	1.02	0.00	3.00
416/32	0.00	0.00	0.00	0.01	0.90	0.00	0.05	0.03	0.00	0.00	0.08	1.92	3.00
296A 15 2	0.00	0.53	0.02	0.46	0.97	0.01	0.07	1.99	0.06	0.00	0.01	0.88	5.00
296A 15 4	0.00	0.52	0.00	0.43	0.94	0.03	0.06	2.03	0.06	0.00	0.00	0.93	5.00
273A 1 5	0.00	1.03	0.15	0.01	0.29	0.00	0.11	0.48	0.00	0.58	0.11	2.25	5.00
273A 1 6	0.00	1.02	0.19	0.01	0.34	0.00	0.11	0.48	0.00	0.55	0.12	2.17	5.00
296 6 1	0.00	0.04	0.00	0.04	2.08	0.00	0.08	1.18	0.56	0.00	0.00	0.00	4.00
296A 9 2	0.00	0.01	0.00	0.01	1.96	0.00	0.13	1.13	0.76	0.00	0.00	0.00	4.00
296B 17	0.00	0.01	0.01	0.03	2.00	0.01	0.11	1.35	0.48	0.00	0.00	0.00	4.00
296B 9 3	0.00	0.05	0.00	0.05	2.05	0.00	0.18	1.05	0.61	0.00	0.00	0.00	4.00
298 1 1	0.00	0.03	0.00	0.02	1.87	0.40	0.38	1.01	0.30	0.00	0.00	0.00	4.00
298 1 2	0.00	0.02	0.00	0.01	2.06	0.02	0.45	1.14	0.31	0.00	0.00	0.00	4.00
298 1 3	0.00	0.02	0.00	0.02	2.08	0.00	0.45	1.19	0.24	0.00	0.00	0.00	4.00
298 1 4	0.01	0.02	0.00	0.01	2.04	0.01	0.39	1.25	0.28	0.00	0.00	0.00	4.00
298A 3 1	0.00	0.03	0.00	0.02	2.02	0.00	0.03	0.88	1.02	0.00	0.00	0.00	4.00
298A 3 4	0.00	0.01	0.00	0.02	2.07	0.02	0.15	1.27	0.46	0.00	0.00	0.00	4.00
298A 3c	0.01	0.02	0.00	0.04	2.04	0.00	0.03	0.99	0.87	0.00	0.00	0.00	4.00
298B 14a	0.00	0.01	0.00	0.01	2.03	0.00	0.16	1.06	0.73	0.00	0.00	0.00	4.00

type chromitites are originally due to extensive stabilization of a Pt_3Fe alloy during precipitation of chromite at magmatic temperatures.

The close co-precipitation of Pt_3Fe with magnesiochromite having the highest oxidation ratio would indicate a sharp drop of the Pt solubility in the Uralian-Alaskan-type magma of Uktus, possibly due to the high iron activity and high oxygen fugacity in the original melt, whereas fS_2 was below sulfide saturation. The absence of Pt phases in magnesiochromite with low iron content and low oxidation ratio apparently supports this conclusion.

The relatively high concentrations of Pt and Ir in Uralian-Alaskan-type chromitites, in general, may reflect a distinctive feature of their parent melts, which is possibly produced by second-stage melting of a depleted and metasomatized mantle source below the subduction zone.

The high-grade Pt ore deposits associated with dunite in Uralian-Alaskan-type complexes (i.e., Nizhny Tagil) often display textural and mineralogical evidence to have formed at relatively low temperature by the action of hydrothermal fluids (Genkin 1997). These deposits may have been generated by the remobilization of a

low-grade Pt "proto-ore" of magmatic origin, such as that described from Uktus.

Acknowledgements We wish to thank the Italian Ministero della Università e della Ricerca Scientifica e Tecnologica for the financial support to this investigation (COFIN 2002). We are grateful to J. Amossé, K.N. Malitch, M. Ohenstetter, D. Ohenstetter, O.A.R. Thalhammer and one unknown referee for useful discussion and critical reading of the manuscript. We also thank B. Lehmann for the editorial review.

References

Amossé J, Allibert M (1993) Partitioning of iridium and platinum between metals and silicate melts: evidence for passivation of the metals depending on fO_2. Geochim Cosmochim Acta 57:2395–2398

Amossé J, Allibert M, Fisher W, Piboule M (1990) Experimental study of the solubility of platinum and iridium in basic silicate melts—implications for the differentiation of platinum-group elements during magmatic processes. Chem Geol 81:45–53

Amossé J, Dablé P, Allibert M (2000) Thermochemical behaviour of Pt, Ir, Rh and Ru vs fO2 and fS2 in a basaltic melt. Implications for the differentiation and precipitation of these elements. Mineral Petrol 68:29–62

Augé T, Johan Z (1988) Comparative study of chromite deposits from Troodos, Vourinos, North Oman and New Caledonia ophiolites. In: Boissonnas J, Omenetto P (eds) Mineral deposits within the European Community. Springer, Berlin Heidelberg New York, pp 267–288

Ballhaus C, Berry RF, Green DH (1991) High pressure experimental calibration of the olivine-orthopyroxene-spinel oxygen geobarometer: implications for the oxidation state of the upper mantle. Contrib Mineral Petrol 107:27–40

Barnes SJ, Naldrett AJ, Gorton MP (1985) The origin of the fractionation of platinum-group elements in terrestrial magmas. Chem Geol 53:303–323

Barnes SJ, Boyd R, Korneliusson A, Nilsson LP, Often M, Pedersen RB, Robins B (1988) The use of mantle normalization and metal ratios in discriminating between the effects of partial melting, crystal fractionation and sulphide segregation on platinum-group elements, gold, nickel and copper: examples from Norway. In: Prichard HM, Potts PJ, Bowles JFW, Cribb SJ (eds) Geo-platinum 87. Elsevier, London, pp 113–143

Betechtin AG (1961) Mikroskopische Untersuchungen an Platinerzen aus dem Ural. N Jb Mineral Abh 97:1–34

Borisov A, Palme H (1997) Experimental determination of the solubility of platinum in silicate melts. Geochim Cosmochim Acta 61:4349–4357

Borisov A, Palme H (2000) Solubility of noble metals in Fe-containing silicate melts as derived from experiments in Fe-free systems. Am Mineral 85:1665–1673

Brenan JM, Andrews D (2001) High-temperature stability of laurite and Ru-Os-Ir alloy and their role in PGE fractionation in mafic magmas. Can Mineral 39:341–360

Cabri LJ, Genkin AD (1991) Re-examination of Pt alloys from lode and placer deposits, Urals. Can Mineral 29:419–425

Cabri LJ, Harris DC, Weiser TW (1996) Mineralogy and distribution of platinum-group mineral (PGM) placer deposits of the world. Explor Mining Geol 5:73–167

Chashchukhin IS, Votyakov SL, Uimin SG (1998) Oxygen thermometry and barometry in chromite-bearing ultramafic rocks: an example of ultramafic massifs on the Urals. II. Oxidation state of ultramafics and the composition of mineralizing fluids. Geochem Int 36:783–791

Fershtater GB, Bea F, Borodina NS, Montero P (1998) Lateral zonation, evolution, and geodynamic interpretation of magmatism of the Urals: new petrological and geochemical data. Petrology 6/5:451–433

Fershtater GB, Bea F, Pushkarev EV, Garuti G, Montero P, Zaccarini F (1999) New data on geochemistry of Platinum Belt of the Urals: contribution to understanding of petrogenesis. Geokhimia 4:1–19

Fominykh VG, Kvostova VP (1970) Platinum content of Ural dunites (in Russian). Dokl Akad Nauk SSSR 191:443–445

Garuti G, Gorgoni C, Sighinolfi GP (1984) Sulfide mineralogy and chalcophile and siderophile element abundances in the Ivrea-Verbano mantle peridotites (Western Italian alps). Earth Planet Sci Lett 70:69–87

Garuti G, Fershtater G, Bea F, Montero P, Pushkarev EV, Zaccarini F (1997a) Platinum-group elements as petrological indicators in mafic-ultramafic complexes of central and southern Urals: preliminary results. Tectonophysics 276:181–194

Garuti G, Oddone M, Torres-Ruiz J (1997b) Platinum-group-element distribution in subcontinental mantle: evidence from the Ivrea zone (Italy) and the Betico-Rifean Cordillera (Spain and Morocco). Can J Earth Sci 34:444–463

Garuti G, Zaccarini F, Moloshag V, Alimov V (1999) Platinum-group minerals as indicators of sulfur fugacity in ophiolitic upper mantle: an example from chromitites of the Ray-Iz ultramafic complex, Polar Urals, Russia. Can Mineral 37:1099–1115

Garuti G, Pushkarev EV, Zaccarini F (2002) Composition and paragenesis of Pt alloys from chromitites of the Uralian-Alaskan type Kytlym and Uktus complexes, northern and central Urals, Russia. Can Mineral 40:357–377

Genkin AD (1997) The sequence and conditions of the formation of platinum-group minerals in the Nizhny Tagil massif (in Russian). Geol Rudnykh Mestorozhdeniy 39:41–48

Hill R, Roeder PL (1974) The crystallization of spinel from basaltic liquid as a function of oxygen fugacity. J Geol 82:709–729

Irvine TN (1967) Chromian spinel as petrogenetic indicator. Part 2. Petrologic implications. Can J Earth Sci 4:71–103

Kaleganov BA, Pushkarev EV (1992) Potassium-argon dating of gabbros of the Uktus and Shabry massifs (in Russian). In: Geology and geochemistry. Ural Branch RAS Year Book 1991, Ekaterinburg, pp 62–64

Lazarenkov VG, Malitch KN (1991) Geochemistry of the ultrabasites of the Konder platiniferous massif (in Russian). Geokhimiya 10:1406–1418

Makeyev AB, Kononkova NN, Kraplya EA, Chernukha FP, Bryanchaninova NI (1997) Platinum group minerals in alluvium of the Northern Urals and Timan: the key to primary sources of platinum. Trans Russian Acad Sci Earth Sci Sect 353:181–184

Makovicky E, Karup-Møller S (2000) Phase relations in the metal-rich portions of the phase system Pt-Ir-Fe-S at 1000 °C and 1100 °C. Mineral Mag 64:1047–1056

Malitch KN (1990) Distribution of platinum-group elements in Aldan-Shield ultrabasic intrusions (in Russian). Geokhimiya 3:425–429

Malitch KN, Thalhammer OAR (2002) Pt-Fe nuggets derived from clinopyroxenite-dunite massifs, Russia: a structural, compositional and osmium-isotope study. Can Mineral 40:395–418

Naldrett AJ, Von Gruenewaldt G (1989) Association of platinum-group elements with chromitites in layered intrusions and ophiolite complexes. Econ Geol 84:180–187

Nixon GT, Cabri LJ, Laflamme JHG (1990) Platinum-group-element mineralization in lode and placer deposits associated with the tulameen Alaskan-type complex, British Columbia. Can Mineral 28:503–535

Pushkarev EV (2000) Petrology of the Uktus dunite-clinopyroxenite-gabbro massif (the Middle Urals) (in Russian). Monogr Russian Acad Sci Ural Branch, Inst Geol Geochem, Ekaterimburg

Pushkarev EV, Puchkova AV (1991) The Uktus mafic-ultramafic massif (Middle Urals) (in Russian). In: Geology and geo-

chemistry. Ural Branch RAS Year Book 1990, Sverdlovsk, pp 35–37
Pushkarev EV, Gulayeva TY, Palgueva GV, Petrisheva VG, Sherstobitova DA (1994) The dunites of the Uktus massif (in Russian). In: Geology and geochemistry. Ural Branch RAS Year Book 1993, Sverdlovsk, pp 73–79
Pushkarev EV, Anikina YeV, Garuti G, Zaccarini F, Cabella R (1999) Geikielite (Mg-ilmenite) in association with Cr-spinel and platinoids from the Uktus massif dunite, Middle Urals: genetic implications. Dokl Earth Sci 369A 9:1220–1223
Razin LV (1976) Geologic and genetic features of forsterite dunites and their platinum-group mineralization. Econ Geol 71:1371–1376
Roeder PL (1994) Chromite: from the fiery rain of chondrules to the Kilauea Iki lava lake. Can Mineral 32:729–746
Skinner BJ, Luke FD, Dill JA, Ellis DE, Hagan HA, Lewis DM, Odell DA, Sverjensky DA, Williams N (1976) Phase relationships in ternary portions of the system Pt-Pd-Fe-As-S. Econ Geol 71:469–1475
St. Louis RM, Nesbitt BE, Morton RD (1986) Geochemistry of platinum-group elements in the Tulameen ultramafic complex, southern British Columbia. Econ Geol 81:961–973
Stockman HW, Hlava PF (1984) Platinum-group minerals in Alpine chromitites from south-western Oregon. Econ Geol 79:491–508
Taylor HP Jr (1967) The zoned ultramaphic complexes of southern Alaska. In: Wyllie PJ (ed) Ultramafic and related rocks. Wiley, New York, pp 97–121
Tistl M (1994) Geochemistry of platinum-group elements of the zoned ultramafic Alto Condoto complex, Northwest Colombia. Econ Geol 89:158–167
Tokarev IF (1922) The dunite-pyroxenite massif of the Uktus mountains (The petrography of Ekaterinburg neighbourhood) (in Russian). Notes Uralian Soc Nature Lovers, Ekaterinburg, vol 38/1, pp 31–41